Polymer 108 (2017) 423–431

Contents lists available at ScienceDirect

Polymer

journal homepage: www.elsevier.com/locate/polymer

Effect of the planar center moiety for a donor-acceptor polymeric electrochrome

Ceylan Doyranlı [a], Betül Çolak [b], Gözde Lacinel [a], Mustafa Can [c], Fatma Baycan Koyuncu [a, b, **], Sermet Koyuncu [b, d, *]

[a] Department of Chemistry, Faculty of Sciences and Arts, Çanakkale Onsekiz Mart University, 17020 Çanakkale, Turkey
[b] Department of Energy Resources and Management, Çanakkale Onsekiz Mart University, 17020 Çanakkale, Turkey
[c] Department of Engineering Sciences, Faculty of Engineering, Izmir Katip Celebi University, Cigli, 35620 Izmir, Turkey
[d] Department of Chemical Engineering, Çanakkale Onsekiz Mart University, Canakkale, Turkey

ARTICLE INFO

Article history:
Received 14 September 2016
Received in revised form
29 November 2016
Accepted 6 December 2016
Available online 8 December 2016

Keywords:
Phenantrene
Electrochromic polymers
Spectroelectrochemistry

ABSTRACT

In this work, phenanthrene centered donor-acceptor monomer; 5,10-bis(4-hexyl-2-thienyl)phenantro [9,10-c][1,2,5]thiodiazole; MES16 was synthesized and then its electrochromic application of corresponding polymer was carried out. 4,7-di(thiophen-2-yl)-2,1,3-benzothiadiazole (TST) was also synthesized as a standard molecule to determine the effect of the planar phenanthrene center on electrochromic performance. Electrochemical properties were elucidated by cyclic voltammetry and then HOMO-LUMO band gaps were calculated by using their oxidation and reduction onset potentials. Finally, electrochromic properties of poly-(MES16) and poly-(TST) were investigated via spectro-electrochemical measurements. DFT calculations exhibit that poly-(MES16) has a high planarity and an intramolecular charge transfer from the polymer backbone-donor to thiadiazole-acceptor subunit. Because of high solid state π–π interactions of the poly-(MES16), a good quality film was obtained corresponding to self-assembly property planar phenantrene center. Owing to this property, electrochromic performance of poly-(MES16) such as response time, stability and ΔT% were better than the standard poly-(TST).

© 2016 Elsevier Ltd. All rights reserved.

1. Introduction

Electrochromic materials can be defined as a reversible change in the absorption, reflection, or transmission of optical radiation upon the material is involved in an electrochemical reductive or oxidative process in the visible, ultraviolet (UV), infrared (IR), and also microwave regimes of the electromagnetic spectrum [1]. First, inorganic semiconductors such as tungsten trioxide (WO_3) [2,3] and iridium dioxide (IrO_2) [4,5] were used as electrochromic material. In comparisons to the inorganic semiconductors, conjugated polymers have some great advantage in electrochromic applications such as high coloration efficiency, low redox potential, high optical contrast, the ability large-area device manufacturing by the solution procesability [6–8]. Besides, the HOMO-LUMO band gap can be adjustment with modification of the chemical structures by means of easily tuning of colors [9]. Due to their advantages, conjugated electrochromic polymers have important applications in technology such as smart-windows [10], electrochromic mirrors [11], anti-glare screens [12], electrochromic display devices [13].

Donor acceptor conjugated polymers have a great importance in electrochromic applications due to their good film forming properties, multi-electrochromic behavior, extended switching stability, fast response time, and low operation potential [14–16]. In 2004, Fred Wudl's group reported the first neutral state green polymer from the thiophene-benzothiadiazole based donor acceptor sturucture [17]. Due to charge tranfer from thiophene-donor to benzothiadizaole-acceptor, a dual absorbance occurs in the visible spectrum to complete the RGB colors. Further, Reynolds' and Toppare's groups improve the electrochomic performance of the system by the chemical modification the donor-acceptor polymeric sturucture [17–20]. Finally, Reynolds et al. has been completed to all CMYK color scale when obtained the yellow colored polymer [21]. All neutral-state RGB and CMYK colored polymers having a

* Corresponding author. Department of Energy Resources and Management, Çanakkale Onsekiz Mart University, 17020 Çanakkale, Turkey.
** Corresponding author. Department of Chemistry, Faculty of Sciences and Arts, Çanakkale Onsekiz Mart University, 17020 Çanakkale, Turkey.
E-mail addresses: fatmabaycan@hotmail.com (F.B. Koyuncu), skoyuncu@comu.edu.tr (S. Koyuncu).

http://dx.doi.org/10.1016/j.polymer.2016.12.016
0032-3861/© 2016 Elsevier Ltd. All rights reserved.

single chromophore demonstrated excellent transmissivity at the oxidized state [22]. Recently, electrochromic performance lifetime and processibility of the polymers can be enhanced by the side chain modification of the polymers [23–25].

The polycyclic aromatic hydrocarbons (PAH) such as phenantrene, anthracene, perylene pyrene, chrysene etc. have significant attention for the optoelectronic technology because of structural rigidity and strong π-stacking interactions on the film surface [26,27]. These PAH derivatives have high chemical stability against environmental conditions and excellent mechanical strength due to consisting of a two-dimensional (2D) sheets of sp^2-hybridized carbon atoms [27]. Because of these useful properties, the PAH have found broad applications in organic light-emitting diodes (OLEDs) [28], organic field effect transistors (OFETs) [29], optical sensors [30], liquid crystals [31]. Furhermore, the PAH have great importance for the organic photovoltaic devices (OPVs) [32,33] and electrochromic materials (ECDs) [34] to improve the morphology on active area of the devices. On the other hand, PAH seems to be a good solution for the stability problem of the optoelectronic devices [35].

Herein, we report the planar phenantrene center effect on the electrochemical, optical, and also electrochromic performance of a donor-acceptor polymer structure. The optical band gap of poly-(5,10-bis(4-hexyl-2-thienyl)phenantro[9,10-c][1,2,5]thiodiazole) (poly-MES16) and poly-(4,7-di(thiophen-2-yl)-2,1,3-benzothiadiazole) (poly-TST) were measured as 2.51 and 1.54 eV, respectively. According to theoretical DFT calculations, a good charge separation was observed at HOMO and LUMO levels of MES16 sturucture. The lamellar morphology could be obtained on the electrochemically prepared polymer film surface due to the solid state π-π* interactions and also self-assembling properties of the poly-(MES16) containing planar phenantrene center. On the other hand, the neutral state color of the polymer was changed from the violet to yellow upon insertion of the phenantrene center instead of phenylene moiety between thiophene-donor and benzazole-acceptor. In comparison to TST standard polymer, poly-(MES16) has much better electrochromic performance in terms of high resistance to over oxidation and high contrast ratio at the visible regime as well as multielectrochromic behavior under applied potential.

2. Experimental

2.1. Materials

All chemicals used without further purification were purchased from commercial suppliers. **TST** was synthesized according to previously published procedures [36]. On the other hand, initial compounds of MES16 (1,2,3 and 4) was prepared according to slightly modified procedure from the literature (Scheme 1) [32].

2.2. Synthesis of 5,10-bis(4-hexyl-2-thienyl)phenantro[9,10-c][1,2,5]thiodiazole (MES16)

4 (0,25 g, 0.5 mmol), 2-(Tri-*n*-butylstannyl)-4-hexylthiophene (0,7 g, 1.5 mmol) and 15 mL toluene were added in a 100 ml flask and stirred under argon atmosphere, for 30 min. After adding the $Pd(PPh_3)_4$ (5 mol %) as a catalyst, the reaction mixture was refluxed at 110 °C for 24 h. Finally, the reaction mixture was cooled and precipitated in 500 mL of ethyl alcohol. Column chromatography [silica gel, $CHCl_3$:Hexane (1:1)] was carried out for the final purification. The pure yellow product (MES16) was obtained and then dried at 40 °C in vacuum oven (Yield: 44%).

FT-IR (cm^{-1}): (C–H aromatic) 3077, 3046; (C–H aliphatic) 2952, 2917, 2851; (C=N) 1611; (C=C phenyl) 1575, 1545, 1567; (C–S thiophene) 741; ^{1}H NMR ($CHCl_3$-d): δ ppm,, 8.61 (s, 2H, Ar-H_c); 7.71 (s, 2H, Ar-H_e); 7.62 (d, 2H, Ar-H_d); 7.21 (d, 2H, Ar-H_a); 6.63 (d,2H, Ar-H_b); 2.58 (t, 4H, Hf); 1.61 (m, 8H, $-C_2H_4$-); 1.22 (m, 8H, $-C_2H_4$-); 0.88 (t, 6H, $-CH_3$).

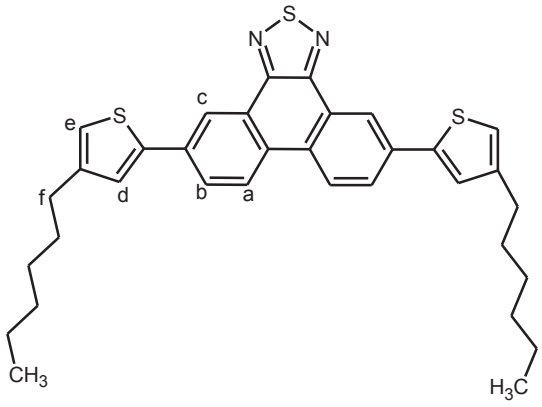

2.3. Instrumentation

Fourier transform infrared spectra (FT-IR) were recorded on a Perkin Elmer FT-IR Spectrum One by using an attenuated total reflectance (ATR) module (4000–650 cm^{-1}). ^{1}H NMR spectra were recorded on a Bruker Advance DPX-400 at 25 °C in deuterated chloroform solutions with tetramethylsilane (TMS) as internal standard. Electrochemical analyses were performed by Biologic SP50 potentiostat–galvanostat system with a platinum disk (0.02 cm^2) as working electrode (WE), Ag wire as reference electrode (RE) and Pt wire as counter electrode (CE). Electrochemical polymerization of MES16 and standard compound TST were realized in a dichloromethane solution consist of 2.0×10^{-3} M monomer and 0.1 M $TBAPF_6$ at 100 mV/s scan rate. The polymer was coated on platinum disc (0.02 cm^2) or ITO/glass electrode (8–12 Ω, 0.8 cm × 5 cm). After the repeating scan in the system, the MES16 and TST polymer thin films were washed with DCM and ACN to eliminate from the electrolyte salt and other impurities. Electrochemical HOMO-LUMO band gap calculated from the oxidation-reduction onset potentials were calibrated against ferrocene redox couple $E^\circ(Fc/Fc^+) = +0.30$ V. UV-vis absorption spectra were recorded by an Analytic Jena Speecord S-600 diode-array spectrophotometer [37]. The optical band gaps (E_g) of polymers were calculated from their absorption onsets [38]. The fluorescence emission spectra were taken by a PTI QM1 fluorescence spectrophotometer. Spectroelectrochemical measurements were carried out to consider absorption spectra of polymer films under applied potential [39]. The color coordinates are determined by three characteristics; luminance (L), hue (a), and saturation (b) in Commission Internationale de l'Elcairage (CIE) system [40]. Analytic Jena UV–vis spectrophotometer with chromameter module was used to determine these characteristics. Surface morphology of the polymer films were investigated at ambient condition and room temperature using a Nanosurf Naio-AFM. To take topographic and phase images, the non-contact mode was used in this system. 20 μm scanner equipped with silicon tips with 15 nm tip-curvature and ITO coated glass substrate was used for measurements. The system was protected with acoustic chamber to avoid electromagnetic noises.

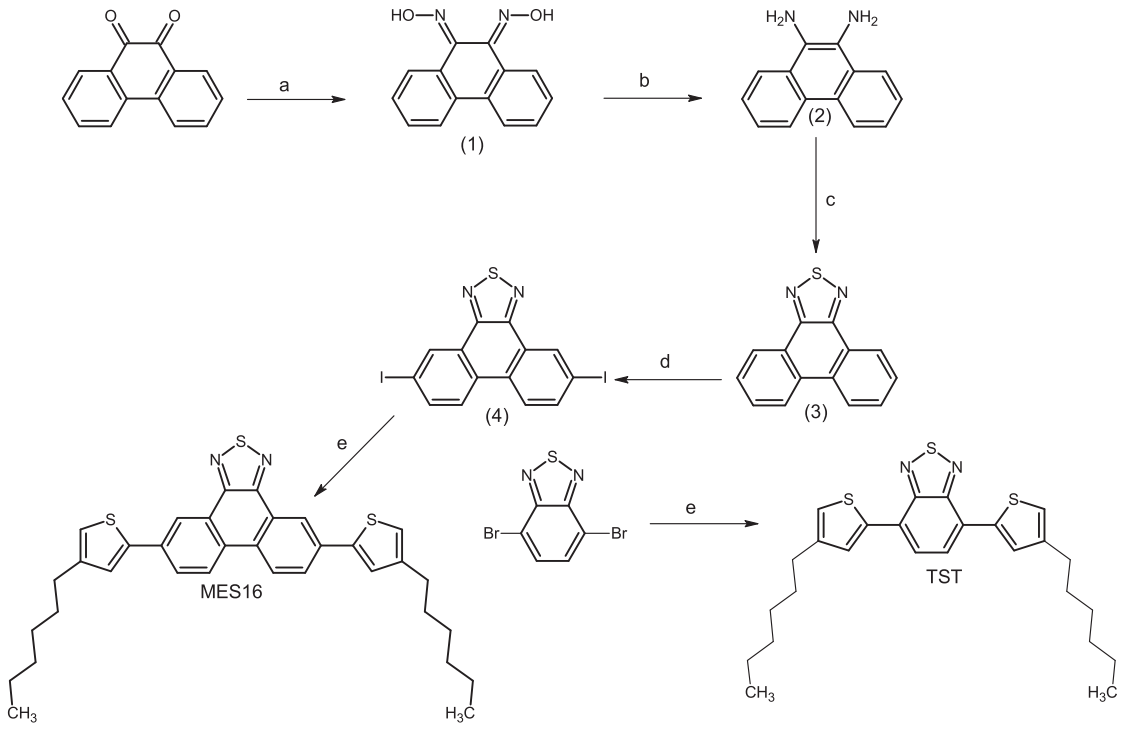

a) $NH_2OH.HCl$ pyridine/EtOH, 130 °C, 3h ; b)EtOH, Pd/C, N_2H_4OH, 80 °C, 24h.; c) DMF, S_2Cl_2, 0 °C, 2h.; d) NIS, H_2SO_4, Ag_2SO_4, rt. 1h; e) 2-(Tri-n-butylstannyl)-4-hexylthiophene*, Toluene, $Pd(PPh_4)$, 110 °C, 24h.*

Scheme 1. Synthetic route to **MES16** monomer.

3. Results and discussion

3.1. Synthesis and characterization

Initial compounds (1, 2, 4 and 4) were obtained according to the literature [32]. Synthesis of MES16 and TST electroactive monomer was obtained by Stille-coupling reaction between 2-(Tri-*n*-butylstannyl)-4-hexylthiophene and dibromo-thiadizole compounds. Then, chemical sturucture of MES16 and TST were clarified by FT-IR, and ^{1}H NMR (Fig. 1).

Repeated scan electrochemical deposition behavior of a solution of 2.0×10^{-3} M of MES16 and TST was investigated in 0.1 M $TBAPF_6$/CH_2Cl_2 electrolyte and 100 mV/s scan rate. Repetitive cycling deposition of MES16 and TST were carried out at 0–1.4 V by potentiodynamic electrochemical process. New semi-reversible oxidation waves were detected at =1.10 V, =1.22 V and =1.16 V and =0.53 V, =1.03 V and =0.78 V in the anodic scan of MES16 and TST, respectively. The peak intensities amplified after each successive cycle during the formation of polymer on the ITO/glass working electrode surface (Fig. 2). Then, poly-(MES16) and TST thin film were washed with ACN and DCM to eliminate the unreacted monomers and/or oligomeric species.

3.2. Optical properties

The optical behaviors of MES16 monomer and TST standard compound were examined by UV-Vis absorption and fluorescence measurements recorded in CH_2Cl_2 (liquid phase). Fig. 2 exhibits the absorption spectra of TST, MES16 and their corresponding polymers. Absorption spectrum of TST shows a characteristic peak at λ_{max} = 310 attributed to π-π* transition of the conjugated system. Besides, resulting from the charge transfer from thiophene-donor to benzathiadiazole-acceptor moieties, a charge transfer band was also observed at λ_{max} = 450. Characteristic π-π* transition band of MES16 was observed at higher wavelength (λ_{max} = 360 nm) due to extended conjugation in the phenanthrene moiety than that of phenylene. Further, the charge transfer band of MES16 was observed at lower wavelength and lower intensity than that of TST because of the electron localization of the condensed phenentrene center. On the other hand, the absorption bands of poly-(MES16) and poly-(TST) bathochromicaly shifted at about 50–100 nm due to increasing π conjugation on the main chain of the structures. The onset wavelength of poly-(TST) was observed at 790 nm corresponding to 260 nm red-shift. MES16 has ring-inner electron localization due to having condensed phenylene rings on the center of the sturucture. Therefore, only a 85 nm red-shift was occurred for poly-(MES16) when compared the MES16 monomer. The optical band gaps were found to be 2.51 eV and 1.54 eV poly-(MES16) and poly-(TST), respectively (Fig. 3).

The fluorescence spectrum of TST exhibited that emission maxima (λ_{max}: 454 nm) shifted 130 nm according to MES16 (λ_{max}: 584 nm) because of a red-shift in absorbance of charge transfer band (Fig. 3). Because of this, the orange color emission turned into cyan upon attaching the phenantrene center unit instead of phenylene (Fig. 3).

3.3. Electrochemical properties

The electrochemical behaviors of TST and MES16 monomers and the corresponding polymers poly-(TST) and poly-(MES16) were examined by cyclic voltammetry (CV). MES16 exhibited an irreversible oxidation peak at = 1.60 V vs. Ag wire in the anodic regime (Fig. 4). However, a semi-reversible oxidation peaks were observed at lower potential for TST standard compound ($E^{ox}_{m,a}$ = 1.12 V

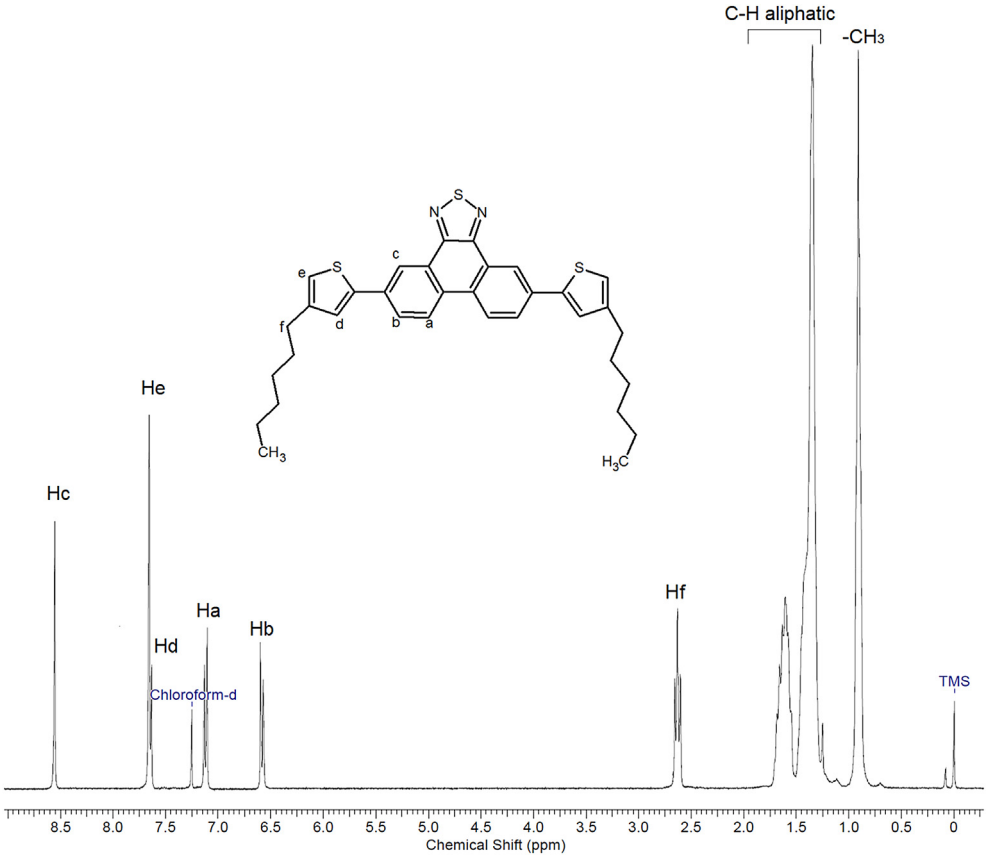

Fig. 1. ^{1}H NMR spevtrum of MES16.

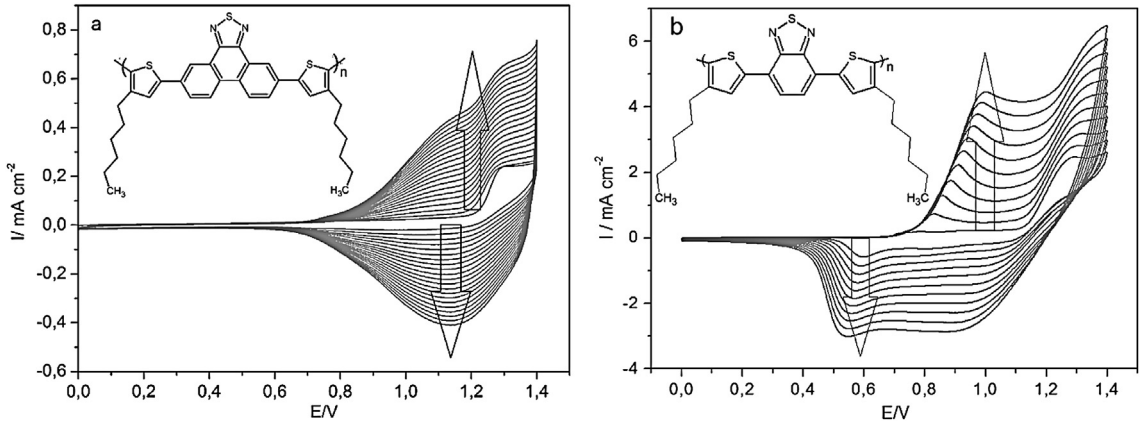

Fig. 2. Electrochemical polymerization of MES16 (a) and TST (b) in 0.1 M $TBAPF_6$ in CH_2Cl_2, scan rate 100 mV/s.

and =0.78 V; =0.95 V). This result indicated that MES16 has ring-inner electron localization due to having triple phenylene rings. After the polymerization process, reversible electrochemical oxidation at lower potential was observed in the poly(MES16) ($E^{ox}_{p,a}$ = 1.27 and =1.19 V; =1.23 V) and poly(TST) ($E^{ox}_{p,a}$ = 1.25 and =1.13 V; =1.19 V).

Due to reduction process of thiadiazole acceptor moiety in the cathodic regime, TST standard molecule exhibits characteristic reversible reduction peaks at =−1.38 and =−1.32 V; =−1.35 V (Fig. 4). The reduction peaks of MES16 were observed at more negative potential ($E^{red}_{m,c}$ = −1.57 and =−1.51 V; =−1.54 V). These slightly higher negative peak potentials for MES16 as the phenanthrene based monomer can be attributed to more localized electron density on the thiadiazole center when compared to TST standard molecule. Hence, MES16 needs a more negative potential for the electron addition into the system. Besides, because of the increasing π-π* conjugation on the polymer backbone at the end of the polymerization, more negative shift was observed. Finally, a reversible reduction peak was observed with a half wave potential ($E^{red}_{p,a}$ = −1.66 V and = −1.74 V; $E^{red}_{p,1/2}$ = −1.70 V for the poly-(MES16). In addition, HOMO-LUMO energy levels and electro-chemical band gaps of MES16, TST and corresponding polymers were given in the Table 1

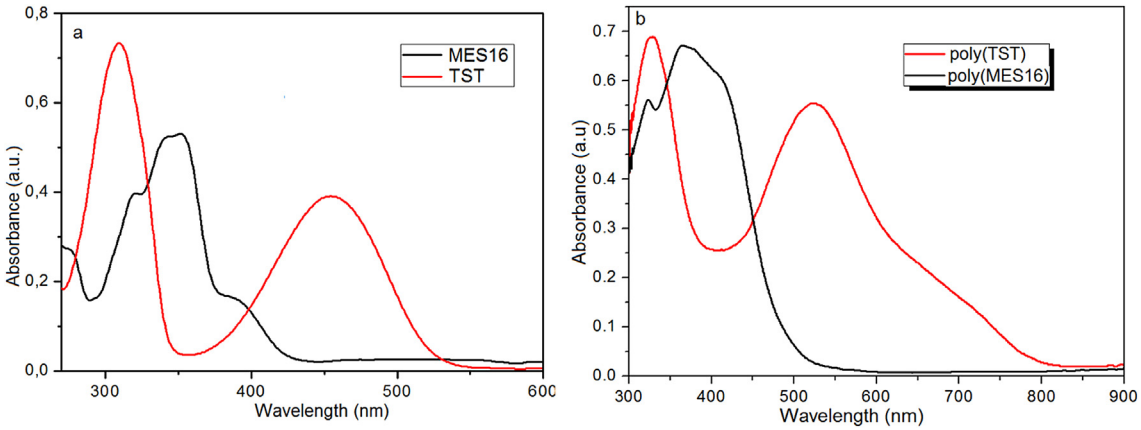

Fig. 3. UV-vis absorption spectra of MES16 and TST (a) and poly(MES16) and poly(TST) (b) in CH_2Cl_2.

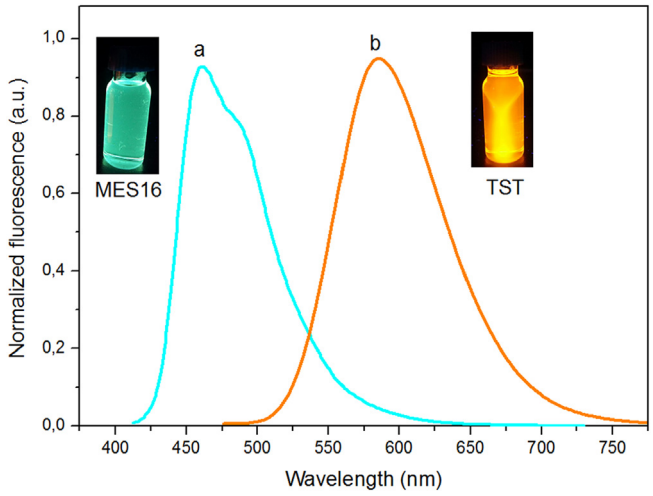

Fig. 4. Fluorescence spectra of **MES16** and **TST** in CH_2Cl_2. Insets: the corresponding photos of compounds with UV light (366 nm).

3.5. DFT calculations

Frontier molecular orbitals have been investigated by Density Functional Theory (DFT) calculations with Spartan10 program at the parameters of B3LYP and 6-31 + G* basis set to get a better understanding of the charge distribution effect on the planar center moiety of donor-acceptor structure. The charge distribution in the frontier molecular orbitals and theoretical calculated HOMO-LUMO levels is shown in Table 2. As displayed in Table 2, HOMO orbitals (HOMO and HOMO-1) are delocalized on the electron-donating main chain thiophenes and neighboring benzene as well as phenantrene. On the other hand, LUMO orbitals (LUMO and LUMO+1) are more localized on the electron-accepting benzo- or phenantrothiadiazole core. The geometry optimized structure exhibited that the MES16 molecule has a higher planarity than that of TST as expected. Because of this property, the charges are more localized at both HOMO and LUMO on the MES16 structure. The HOMO-LUMO band gap calculated by DFT was observed to increase from 2.77 eV to 3.43 eV upon attached phenantrene moiety between 3-hexylthiophene donor and thiadiazole acceptor. On the other hand, all theoretical calculated HOMO-LUMO values are lower than experimental values from the CV and UV-vis measurements.

Table 1
HOMO and LUMO energy levels, electrochemical and optical band gaps of TST, MES16, poly-(TST) and poly-(MES16).

Molecules	Oxidation potential (V)	Reduction potential (V)	HOMO (eV)	LUMO (eV)	Optical band gap (eV)	Electrochemical band gap (eV)
MES16	$E^{ox}_{m,a} = 1.60$	$E^{red}_{m1,a} = -1.57 E^{red}_{m1,c} = -1.51$	−5.66	−3.02	2.93	2.64
Poly(MES16)	$E^{ox}_{p,a} = 1.27 E^{ox}_{p,c} = 1.19$	$E^{red}_{p,a} = -1.74 E^{red}_{p,c} = -1.66$	−5.41	−2.92	2.51	2.49
TST	$E^{ox}_{m,a} = 1.12 E^{ox}_{m,c} = 0.78$	$E^{red}_{m1,a} = -1.38 E^{red}_{m1,c} = -1.32$	−5.44	−3.07	2.34	2.37
Poly(TST)	$E^{ox}_{p,a} = 1.25 E^{ox}_{p,c} = 1.13$	$E^{red}_{p,a} = -1.38 E^{red}_{p,c} = -1.16$	−5.49	−3.20	1.54	2.29

3.4. Surface morphology

Surface morphologies of poly-(TST) and poly-(MES16) films were examined by atomic force microscopy (AFM) (Fig. 5). Polymer films were obtained by potenthiodynamic electrochemical polymerization process. After the coating process, the polymer films were obtained at 100 nm in thickness. Owing to the planar structure of phenanthrene center, solid state π-π* interaction is increased and the lamellar morphology could be obtained due to the self-assembling properties of poly-(MES16) (Fig. 5) Besides poly-(MES16) film has more smooth surface than that of Poly-(TST) (Fig. 5). The roughness values of the polymer films were calculated to the 6 nm for poly-(MES16) and 14 nm for poly-(TST), respectively (see Fig. 6).

3.6. Spectro-electrochemical properties

The electrochromic behavior of poly-(TST) and poly-(MES16) films were investigated by spectro-electrochemical measurements using a diode-array spectrophotometer under applied potential [39]. During to anodic scan of poly-(TST) film (0–1.6 V), the valance band-conduction bands (π→π* transition) at about 325 and 525 nm started to decrease, whereas a new absorption band at 825 nm intensified in the NIR region by the increased positive potential. The purple color (L*: 38.9; a: 7.1; b: −14,9) of the film was bleached and converted to light blue (L*: 64.2; a: −0.4; b: −15.2)

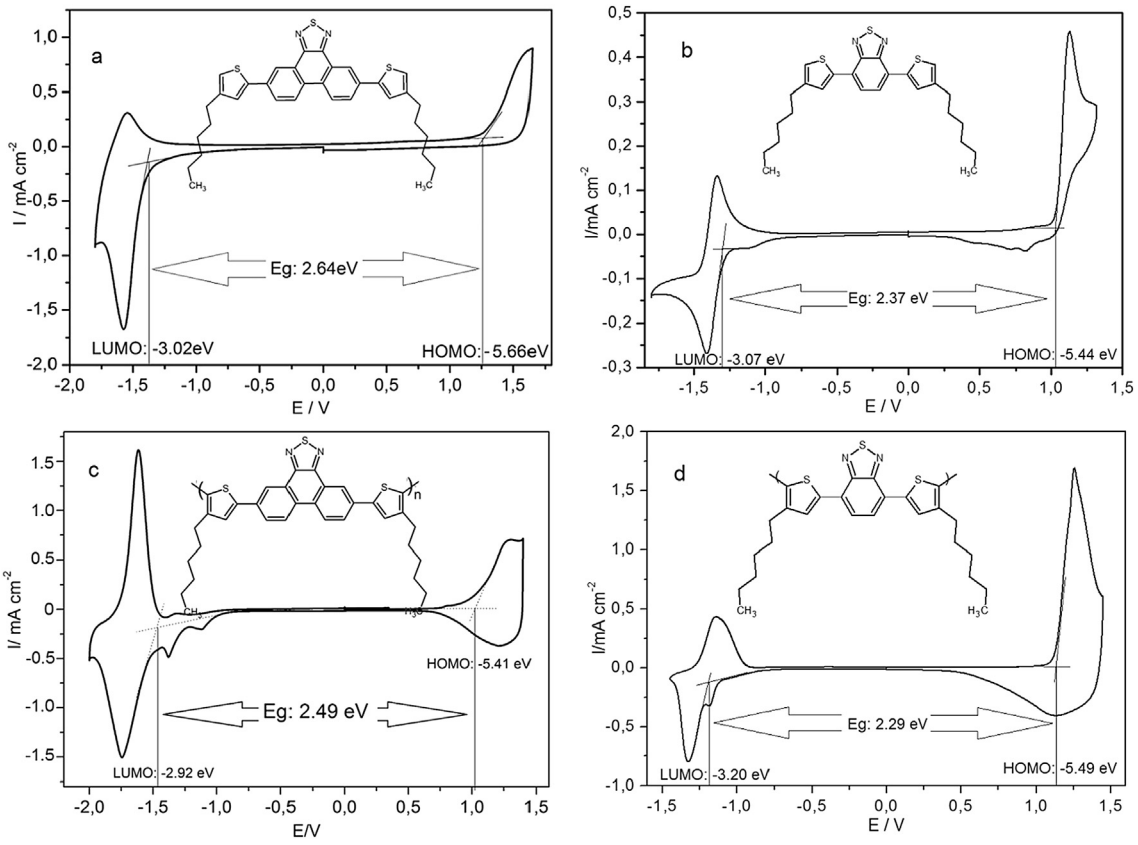

Fig. 5. Cyclic voltamogram of (a) TST, (b) MES16, (c) poly-(TST), (d) poly-(MES16) in 0.1 M $TBAPF_6$/DCM, scan rate 100 mV/s.

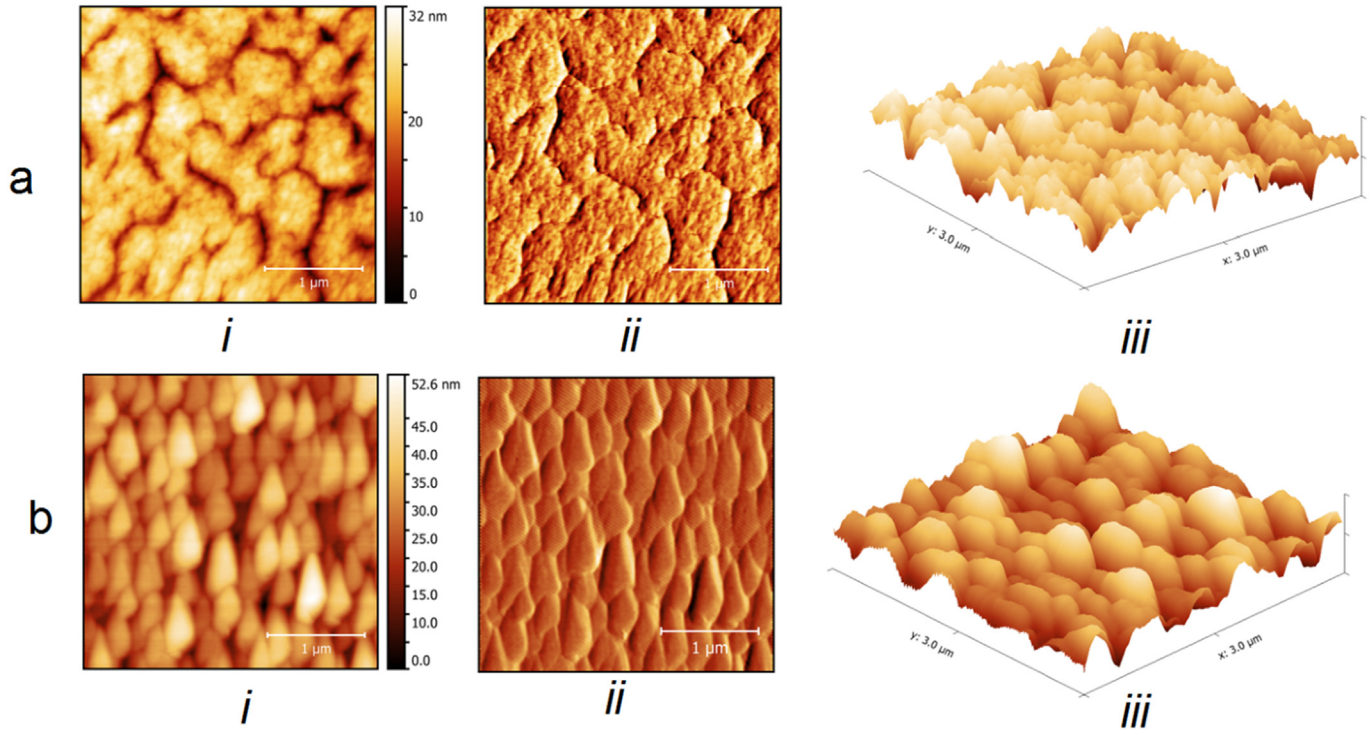

Fig. 6. AFM images of a) poly-(MES16) and b) poly-(TST) films; i) height image, ii) phase image, and iii) topography image.

Table 2
Molecular orbital diagrams of the HOMO and LUMO levels of MES16 and TST.

	MES16	TST
LUMO+1	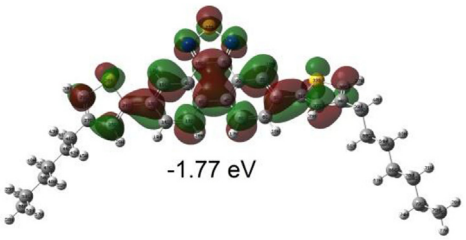	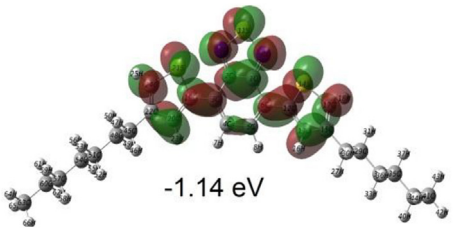
LUMO	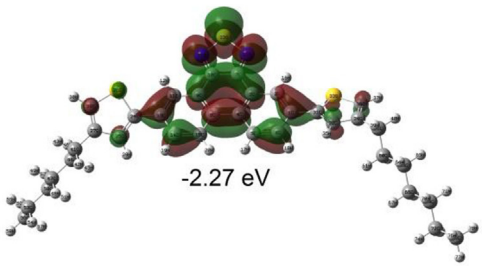	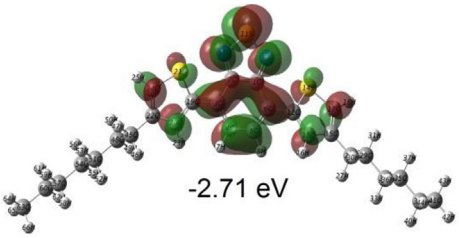
HOMO	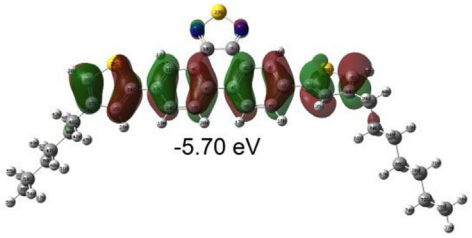	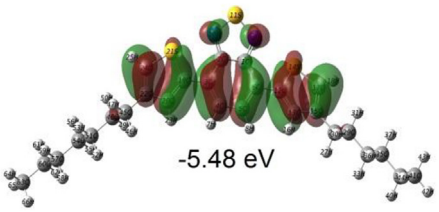
HOMO-1	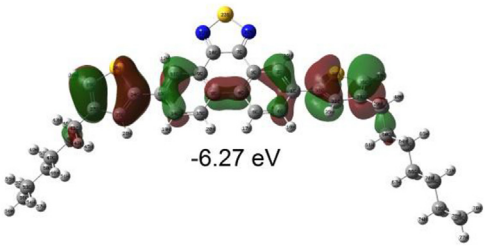	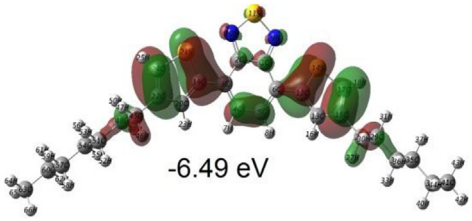
Theoretical Band Gap (E_g)	3.43 eV	2.77 eV

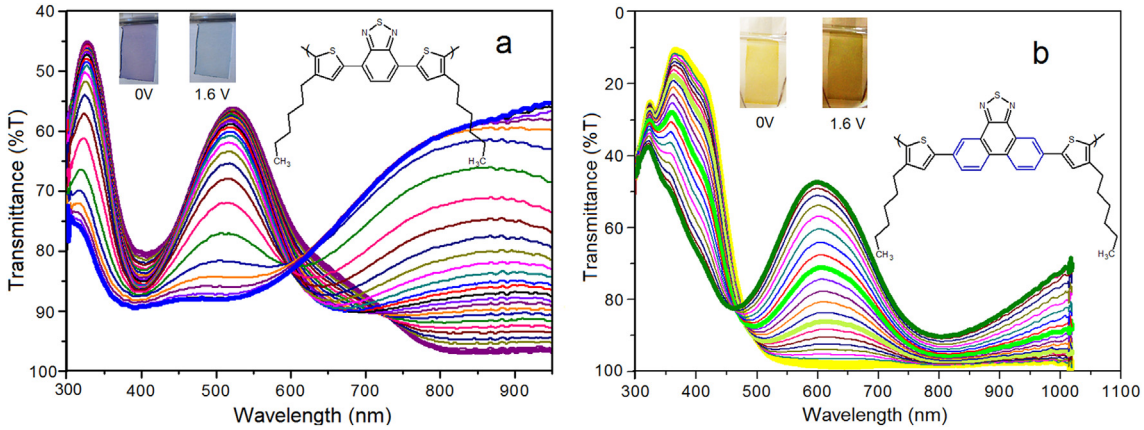

Fig. 7. UV-Vis spectra and the color changes during the applied potential of **poly-(TST) (a) and poly-(MES16) (b)** films on ITO/glass surface in 0.1 M $TBAPF_6$/ACN.

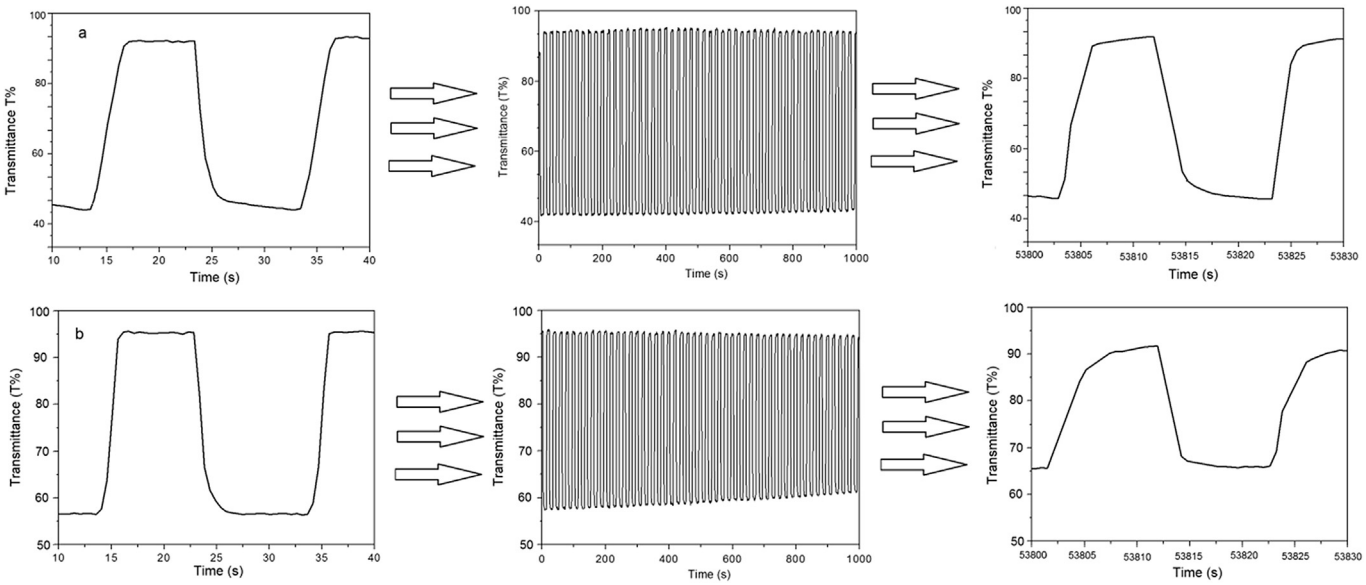

Fig. 8. Electronic absorption spectra for poly-(MES16) (a) and poly-(TST) (b) films upon p doping between 0 and 1.6 V in a monomer-free 0.1 M $TBAPF_6$/ACN solution.

during the oxidation process (Fig. 7a).

It is observed that the neutral state color of the polymer film converted from purple to yellow upon attaching the phenantrene moiety instead of phenylene on the conjugated polymer main chain. Upon oxidation of poly-(MES16), an absorption band at 370 nm corresponds to valence band-conduction band ($\pi \rightarrow \pi^*$ transition) started to decrease and the new absorption bands intensified at 600 nm which indicated the formation of polarons and bipolarons on the polymer backbone. Consequently, yellow color of the poly-(MES16) film (L^*:83.9; a: −7.6; b: 33.8) at the neutral state turned to many different tones of green color (L^*:72.3; a: −11.6; b: 63.1—L^*:72.3; a: −11.6; b: 63.1—L^*:52.6; a: −9.7; b: 41.1) by intensified the absorption bands in the visible regime (Fig. 7b).

Kinetic performances of poly-(MES16) and poly-(TST) were investigated by the square-wave voltammetry which is observed difference of transmittance at the point of absorption maxima with against to time while applying potential between redox states of polymers with a residence time of 10 s (Fig. 8). There are a few parameters to determine the electrochromic performance of the polymer films such as stability and percentage transmittance change (ΔT%) against to applied potential as well as response time. ΔT% and response time of poly-(MES16) and poly-(TST) were determined between 0 and 1.6 V with switching time of 10 s. As a result of these measurements, ΔT% values of poly(MES16) (at 600 nm) and poly-(TST) (at 900 nm) were measured as 47% and 40%, respectively (Fig. 8). According the stability test under applied potential after about 5000 cycles, poly-(MES16) and poly-(TST) preserve the optical activity as 98% and 71%, respectively. The oxidation and reduction response times were also calculated as 3.2 and 3.4 s for poly-(MES16), 2.1 and 2.8 s for poly-(TST), respectively. This phenomenon can be explained that slower charge exchange between electrolyte solution and polymer chain was occurred during the oxidation process due to the electron localization in the phenanthrene ring at the oxidized state.

Coloration efficiency (CE) is another important parameter for the electrochromic applications. CE was calculated by this equation: $CE = \Delta OD/Q_d$ and $\Delta OD = \log (T_{colored}/T_{bleached})$ [$T_{bleached}$: Transmittance at neutral state, $T_{colored}$:Transmittance at oxidized state and Q_d: Injected/ejected charge between redox states [41]. According to this equation, CE values of poly-(MES16) and poly-(TST) were calculated as 228 and 132 $cm^2\ C^{-1}$, respectively. It can be clearly observed that CE value of poly-(MES16) is approximately two times greater than that of poly-(TST). Considering all data, electrochromic performance of the poly-(MES16) was better in comparison to poly-(TST).

4. Conclusion

Herein, we have reported the effect of planar center unit on the electrochromic performance of the conjugated polymers. It has been observed that thin film morphologies, optical and the electrochemical properties were greatly influenced from the presence of the phenantrene center unit on the conjugated structure. According to DFT calculations, the charges are more localized at both HOMO and LUMO on the MES16 when compared with the TST standart molecule. MES16 electroactive monomer was electrochemically polymerized onto transparent ITO/glass surface to give a quite stable multi-electrochromic polymer with a high contrast ratio in the visible regime (ΔT = 47% at 600 nm). In comparison to poly-(TST) as a standard polymer, poly-(MES16) has much better electrochromic performance. Owing to a high contrast ratio in the visible regime and an impressive electrochemical stability against to applied redox potentials, poly-(MES16) is a possible good candidate for the electrochromic applications.

Acknowledgements

We also gratefully acknowledge to Scientific and Technical Research Council of Turkey (TUBITAK, project #: 113Z581) for financial support.

References

[1] P.M. Beaujuge, J.R. Reynolds, Color control in pi-conjugated organic polymers for use in electrochromic devices, Chem. Rev. 110 (1) (2010) 268–320.
[2] C.G. Granqvist, Progress in electrochromics: tungsten oxide revisited, Electrochim Acta 44 (18) (1999) 3005–3015.
[3] P. Delichere, P. Falaras, A.H. Goff, Wo3 anodic films in organic medium for electrochromic display devices, Sol. Energ Mater 19 (3–5) (1989) 323–333.
[4] W.C. Dautremontsmith, L.M. Schiavone, S. Hackwood, G. Beni, J.L. Shay, Electrochromic cells with iridium oxide display electrodes, Solid State Ionics 2 (1) (1981) 13–18.
[5] S. Hackwood, W.C. Dautremontsmith, G. Beni, L.M. Schiavone, J.L. Shay,

Volume changes induced by the electrochromic process in sputtered iridium oxide-films, J. Electrochem Soc. 128 (6) (1981) 1212–1214.
[6] I. Schwendeman, R. Hickman, G. Sonmez, P. Schottland, K. Zong, D.M. Welsh, J.R. Reynolds, Enhanced contrast dual polymer electrochromic devices, Chem. Mater 14 (7) (2002) 3118–3122.
[7] A.A. Argun, A. Cirpan, J.R. Reynolds, The first truly all-polymer electrochromic devices, Adv. Mater 15 (16) (2003) 1338.
[8] M.R. Huang, T. Tao, X.G. Li, Q.C. Gong, An electrochromic film device to teach polymer electrochemical physics, Am. J. Phys. 75 (9) (2007) 839–843.
[9] L. Zophel, V. Enkelmann, K. Mullen, Tuning the HOMO-LUMO gap of pyrene effectively via donor-acceptor substitution: positions 4,5 versus 9,10, Org. Lett. 15 (4) (2013) 804–807.
[10] M. Andrei, A. Roggero, L. Marchese, S. Passerini, Highly conductive solid polymer electrolyte for smart windows, Polymer 35 (17) (1994) 3592–3597.
[11] K. Tajima, H. Hotta, Y. Yamada, M. Okada, K. Yoshimura, Electrochromic switchable mirror glass with controllable reflectance, Appl. Phys. Lett. 100 (9) (2012).
[12] J.A. Ferwerda, A. Stillwell, H. Hovagimian, E.M.K. Williams, Perception of sparkle in anti-glare display screens, J. Soc. Inf. Disp. 22 (2) (2014) 129–136.
[13] O. Bohnke, C. Bohnke, Solid-state electrochromic display device, P Soc. Photo-Opt Ins. 1126 (1989) 40–46.
[14] T. Sugimoto, T. Nagatomi, H. Ando, Z. Yoshida, Redox-active Thieno[3,2-B] Thiophene as a novel, 3-color electrochromic system, Angewandte Chemie-International Ed. Engl. 27 (4) (1988) 560–561.
[15] X.G. Li, H.Y. Wang, M.R. Huang, Synthesis, film-forming, and electronic properties of o-phenylenediamine copolymers displaying an uncommon tricolor, Macromolecules 40 (5) (2007) 1489–1496.
[16] X.G. Li, M.R. Huang, W. Duan, Y.L. Yang, Novel multifunctional polymers from aromatic diamines by oxidative polymerizations, Chem. Rev. 102 (9) (2002) 2925–3030.
[17] G. Sonmez, C.K.F. Shen, Y. Rubin, F. Wudl, A red, green, and blue (RGB) polymeric electrochromic device (PECD): the dawning of the PECD era, Angew. Chem. Int. Ed. 43 (12) (2004) 1498–1502.
[18] R.M. Walczak, J.K. Leonard, J.R. Reynolds, Processable, electroactive, and aqueous compatible poly(3,4-alkylenedioxypyrrole)s through a functionally tolerant delodination condensation polymerization, Macromolecules 41 (3) (2008) 691–700.
[19] P.M. Beaujuge, S. Ellinger, J.R. Reynolds, Spray processable green to highly transmissive electrochromics via chemically polymerizable donor-acceptor heterocyclic pentamers, Adv. Mater 20 (14) (2008) 2772.
[20] G.E. Gunbas, A. Durmus, L. Toppare, Could green be greener? Novel donor-acceptor-type electrochromic polymers: towards excellent neutral green materials with exceptional transmissive oxidized states for completion of RGB color space, Adv. Mater 20 (4) (2008) 691.
[21] C.M. Amb, J.A. Kerszulis, E.J. Thompson, A.L. Dyer, J.R. Reynolds, Propylene-dioxythiophene (ProDOT)-phenylene copolymers allow a yellow-to-transmissive electrochrome, Polym. Chem-Uk 2 (4) (2011) 812–814.
[22] A.L. Dyer, E.J. Thompson, J.R. Reynolds, Completing the color palette with spray-processable polymer electrochromics, Acs Appl. Mater Inter 3 (6) (2011) 1787–1795.
[23] P.J. Shi, C.M. Amb, A.L. Dyer, J.R. Reynolds, Fast switching water processable electrochromic polymers, Acs Appl. Mater Inter 4 (12) (2012) 6512–6521.
[24] P.M. Beaujuge, C.M. Amb, J.R. Reynolds, A side-chain defunctionalization approach yields a polymer electrochrome spray-processable from water, Adv. Mater 22 (47) (2010) 5383.
[25] M.T. Otley, F.A. Alamer, Y.M. Zhu, A. Singhayiranon, X.Z. Zhang, M.F. Li, A. Kumar, G.A. Sotzing, Acrylated poly(3,4-propylenedioxythiophene) for enhancement of lifetime and optical properties for single-layer electrochromic devices, Acs Appl. Mater Inter. 6 (3) (2014) 1734–1739.
[26] B. Korchowiec, Y. Corvis, T. Viitala, C. Feidt, Y. Guiavarch, C. Corbier, E. Rogalska, Interfacial approach to polyaromatic hydrocarbon toxicity: phosphoglyceride and cholesterol monolayer response to phenantrene, anthracene, pyrene, chrysene, and benzo[a]pyrene, J. Phys. Chem. B 112 (43) (2008) 13518–13531.
[27] A. Mateo-Alonso, Pyrene-fused pyrazaacenes: from small molecules to nanoribbons, Chem. Soc. Rev. 43 (17) (2014) 6311–6324.
[28] K.R.J. Thomas, N. Kapoor, M.N.K.P. Bolisetty, J.H. Jou, Y.L. Chen, Y.C. Jou, Pyrene-fluorene hybrids containing acetylene linkage as color-tunable emitting materials for organic light-emitting diodes, J. Org. Chem. 77 (8) (2012) 3921–3932.
[29] K. Oniwa, H. Kikuchi, H. Shimotani, S. Ikeda, N. Asao, Y. Yamamoto, K. Tanigaki, T.N. Jin, 2-Positional pyrene end-capped oligothiophenes for high performance organic field effect transistors, Chem. Commun. 52 (26) (2016) 4800–4803.
[30] B.J. Basu, A. Thirumurugan, A.R. Dinesh, C. Anandan, K.S. Rajam, Optical oxygen sensor coating based on the fluorescence quenching of a new pyrene derivative, Sens. Actuat B-Chem 104 (1) (2005) 15–22.
[31] N. Sebastian, M.R. de la Fuente, D.O. Lopez, M.A. Perez-Jubindo, J. Salud, M.B. Ros, Overall dielectric study on the odd members of a highly nonsymmetric pyrene-based series of liquid crystal dimers, J. Phys. Chem. B 117 (46) (2013) 14486–14496.
[32] S. Song, S. Park, S. Kwon, B.H. Lee, J.Y. Shim, J. Lee, S.H. Park, Y. Jin, I. Kim, K. Lee, H. Suh, Synthesis and photovoltaic property of copolymers with phenanthrothiadiazole moiety, Sol. Energ Mat. Sol. C 105 (2012) 229–236.
[33] O.P. Lee, A.T. Yiu, P.M. Beaujuge, C.H. Woo, T.W. Holcombe, J.E. Millstone, J.D. Douglas, M.S. Chen, J.M.J. Frechet, Efficient small molecule bulk heterojunction solar cells with high fill factors via pyrene-directed molecular self-assembly, Adv. Mater 23 (45) (2011) 5359.
[34] E. Sefer, S.O. Hacioglu, M. Tonga, L. Toppare, A. Cirpan, S. Koyuncu, A novel near-IR effective pyrene-based donor-acceptor electrochrome, Macromol. Chem. Phys. 216 (8) (2015) 829–836.
[35] Y.C. Kung, S.H. Hsiao, Novel luminescent and electrochromic polyhydrazides and polyoxadiazoles bearing pyrenylamine moieties, Polym. Chem-Uk 2 (8) (2011) 1720–1727.
[36] S.P. Wen, J.N. Pei, P.F. Li, Y.H. Zhou, W.D. Cheng, Q.F. Dong, Z.F. Li, W.J. Tian, Synthesis and photovoltaic properties Of Low-Bandgap 4,7-Dithien-2-yl-2,1,3-Benzothiadiazole-Based Poly(heteroarylenevinylene)s, J. Polym. Sci. Pol. Chem. 49 (12) (2011) 2715–2724.
[37] C.M. Cardona, W. Li, A.E. Kaifer, D. Stockdale, G.C. Bazan, Electrochemical considerations for determining absolute frontier orbital energy levels of conjugated polymers for solar cell applications, Adv. Mater 23 (20) (2011) 2367–2371.
[38] A.O. Patil, A.J. Heeger, F. Wudl, Optical-properties of conducting polymers, Chem. Rev. 88 (1) (1988) 183–200.
[39] W. Kaim, J. Fiedler, Spectroelectrochemistry: the best of two worlds, Chem. Soc. Rev. 38 (12) (2009) 3373–3382.
[40] B.C. Thompson, P. Schottland, K.W. Zong, J.R. Reynolds, In situ colorimetric analysis of electrochromic polymers and devices, Chem. Mater 12 (6) (2000) 1563–1571.
[41] R.J. Mortimer, J.R. Reynolds, In situ colorimetric and composite coloration efficiency measurements for electrochromic Prussian blue, J. Mater Chem. 15 (22) (2005) 2226–2233.